Int. J. Electrochem. Sci., 6 **(2011)** 404 - 418

International Journal of
ELECTROCHEMICAL
SCIENCE
www.electrochemsci.org

Corrosion Behavior of Ni-Al-Cu Alloys in Simulated Human Body Solution

I. E. Castañeda[1], J.G. Gonzalez-Rodriguez[2], G. Dominguez-Patiño[2], R. Sandoval-Jabalera[3], M.A.Neri-Flores[1], JG. Chacon-Nava[1], A. Martinez-Villafañe[1]*

[1] Centro de Investigación en Materiales Avanzados. S.C.- Complejo Industrial Chihuahua Chihuahua, Chih. Mexico
[2] UAEM-Centro de Investigación en Ingeniería y Ciencias Aplicadas, Av. Universidad 1001, Col. Chamilpa, Cuernavaca Mor., Mexico
[3] UACH, Facultad de Ingeniería. Chihuahua, Chih. México
[*]E-mail: martinez.villafane@cimav.edu.mx

Received: 9 November 2010 / *Accepted:* 15 December 2010 / *Published:* 1 February 2011

An investigation about the corrosion resistance of Ni-Al-Cu intermetallic alloys in simulated human body fluid environments has been carried out by using electrochemical techniques. Tested alloys included 50 (wt %) Ni-(20 and 25) Al-(20 and 25) Cu using the Hank´s solution. For comparison, 316L type stainless steel has also been evaluated. Electrochemical techniques included potentiodynamic polarization curves, linear polarization resistance (LPR), electrochemical impedance spectroscopy (EIS), and electrochemical noise measurements, EN. Different techniques have shown that, generally speaking, Ni-Al-Cu alloys showed a lower corrosion resistance than conventional 316L type stainless steel only during a few days. Their corrosion resistance decreased as the Cu content in the alloy decreased. The alloys were susceptible to pitting type of corrosion on the γ'-$(Ni, Cu)_3Al$ Cu-rich phases.

Keywords: Corrosion, human body, electrochemical impedance, electrochemical noise.

1. INTRODUCTION

Traditional biomedical metallic materials such as stainless steels and Ti and Ti alloys have played an essential role to repair or replace diseased or damaged bone tissues. However, after their implantation in human bodies, sometimes mechanical failure occurs and tissue inflammation may happen, which become dissatisfactory and insufficient for their biomedical applications [1]. Corrosion and surface film dissolution are two responsible mechanisms for introducing ions in the body from the implants. Extensive release of metal ions from human body implants can result in adverse biological

reactions and even lead to mechanical failure of the device. Most of the used materials for human implants include 316L type stainless steels [2-6], titanium-base alloys [7-11], or cobalt-base alloys [12-16]. Aluminides are receiving a considerable attention relative to their aqueous corrosion properties in acidic, basic, chloride and sulfur-compound solutions [17-20]. Among the novel room temperature applications of these materials, their potential use such as biomaterials or in applications in a seawater atmosphere can be considered [17-20]. Garcia-Alonso, for instance, found that the corrosion rate of Fe_3Al-type intermetallic under three different heat treatments were within the same order of magnitude than that for 316L type stainless steel in a simulated human body fluid [17] whereas Lopez [18] obtained similar results with another iron-base alloy.

Nickel aluminide, NiAl, is an intermetallic compound that is formed as a result of the ordering of nickel and aluminum atoms on the f.c.c. unit cell. As a promising intermetallic, it can be used in both low and high temperature due to its high melting point, low density, and excellent thermal conductivity. They have excellent corrosion resistance in most environments due to the establishment of an external Al_2O_3 layer. In addition to this, they offer better mechanical properties such as strength, and potentially lower costs than other materials used as human implants, not only as permanent hip prosthesis, but also as temporal dental brackets. However, the rather low ductility at low temperature has hindered the development of these intermetallic materials. Ternary additions to Ni-Al have been investigated by several researchers [19-21], and it has been reported, for instance, that Cu additions replace the atoms of Al. During solidification of Ni-Al alloys with ternary additions of Fe, Co, Cr or Cu, ternary elements were distributed into γ phase; in particular, Cu additions induced formation of γ phase [22], and small amounts of Cu destabilized the β phase and induced the β´ martensite transformation. The aqueous, low temperature corrosion resistance of Ni-Al is of concern for high temperature applications because these materials will not always be operating at high temperatures but also al low temperatures, and corrosion damage during fabrication or maintenance could lead to catastrophic failures during service. Thus, the goal of this work is to investigate the effect of alloying with Cu a NiAl alloy on its corrosion resistance in human body solutions for their potential use as biomaterials.

2. EXPERIMENTAL PROCEDURE

Chemical composition of tested Ni-Al-Cu alloys is given on table 1. The alloys were vacuum induction melted at 1700 °C and casted in copper chill molds to produce ingots 0.002 m thick, 0.020 m wide, and 0.050 m long.

Table 1. Chemical composition of tested materials (wt %)

Material	Ni	Al	Cu
M1	50	25	25
M2	50	30	20

Ingots were then heat treated under a high-purity argon atmosphere at 550 °C (24 h) and cooled in air until room temperature was reached. For comparison, some tests were performed on a 316L type stainless steel also. To perform the corrosion test experiments, these specimens were polished with diamond paste to a 0.1 μm finish. Electrochemical experiments were performed using an ACM Instruments potentiostat controlled by a personal computer. Potentiodynamic polarization curves were obtained by varying the applied potential from –500 mV with respect to the free corrosion potential, E_{corr}, up to +600 mV at a rate of 1mV s^{-1}. Before the experiments, the E_{corr} value was measured during approximately 30 minutes, until it was stable. All potentials were measured using a Saturated Calomel Electrode (SCE) as reference electrode. The counter electrode was a platinum wire. Linear polarization resistance measurements, LPR, were performed by polarizing the specimen from +10 to -10 mV, with respect to E_{corr}, at a scan rate of 1 mV s^{-1} every day during 16 days. All tests were performed at 37 ± 2 °C. Electrochemical impedance spectroscopy tests, EIS, were carried out at E_{corr} by using a signal with amplitude of 10 mV and a frequency interval of 0.1 Hz-30 kHz. Finally, electrochemical noise measurements (EN) in both current and potential were recorded using two identical working electrodes and a SCE. Electrochemical noise measurements were made by recording simultaneously the potential and current fluctuations at a sampling rate of 1 point per second for a period of 1024 seconds. A fully automated zero resistance ammeter (ZRA) from ACM instruments was used in this case. Removal of the DC trend from the raw noise data was the first step in the noise analysis when needed. To accomplish this, a least square fitting method was used. Finally, the noise resistance, $R_{n,}$ was then calculated as the ratio of the potential noise standard deviation, σ_v, over the current noise standard deviation, σ_i. The aqueous solution used included the Hank's solution with a chemical composition as given on table 2.

Table 2. Chemical composition of Hank's solution (g/l).

NaCl	$CaCl_2$	KCl	Glucose	$NaHCO_3$	$MgCl_2.6H_2O$	$Na_2HPO_4.2H_2O$	KH_2PO_4	$MgSO_47H_2O$
8	0.14	0.4	1	0.35	1	0.06	0.06	0.06

3. RESULTS AND DISCUSSION

Fig. 1 shows the microstructures of the Ni-Al-Cu alloys containing 25 and 20 % Cu respectively. The microstructure of both alloys consists basically of the polygonal β-(Ni, Cu)Al, white phase, together with the black, γ'-$(Ni, Cu)_3Al$ phase, along the β-(Ni, Cu)Al grain boundaries. The average grain size was between 15-20 μm. No other precipitates could be observed.

Potentiodynamic polarization curves for the two Cu-containing Ni-Al alloys and 316L type stainless steel are given on Fig. 2. It can be seen that the three alloys exhibited an active-to-passive behavior, where the noblest E_{corr} value was for 316L stainless steel, close to -210 mV, whereas the most active value was for the 20% Cu-containing Ni-Al alloy, -532 mV, which is expected due to the lower Cu content in the alloy. The lowest corrosion current density value was for alloy containing 25%

Cu, 2.75 x 10^{-5} mA cm^{-2}, whereas the highest value was for 316L type stainless steel, 1.5 X 10^{-3} mA cm^{-2}, very close to that obtained for the 20% Cu, 2.75 x 10^{-5} mA cm^{-2}. Additionally, the 20% Cu-containing alloy exhibited the lowest pitting potential value, E_{pit}, (-160 mV) whereas the highest value, 330 mV, was for 316L stainless steel, although both alloys showed similar passive current density values, i_{pp}. This data show a greater susceptibility to pitting corrosion of Ni-Al-Cu intermetallics than that for 316L type stainless steel. Repasivation tests were not conducted. Table 3 summarizes these values.

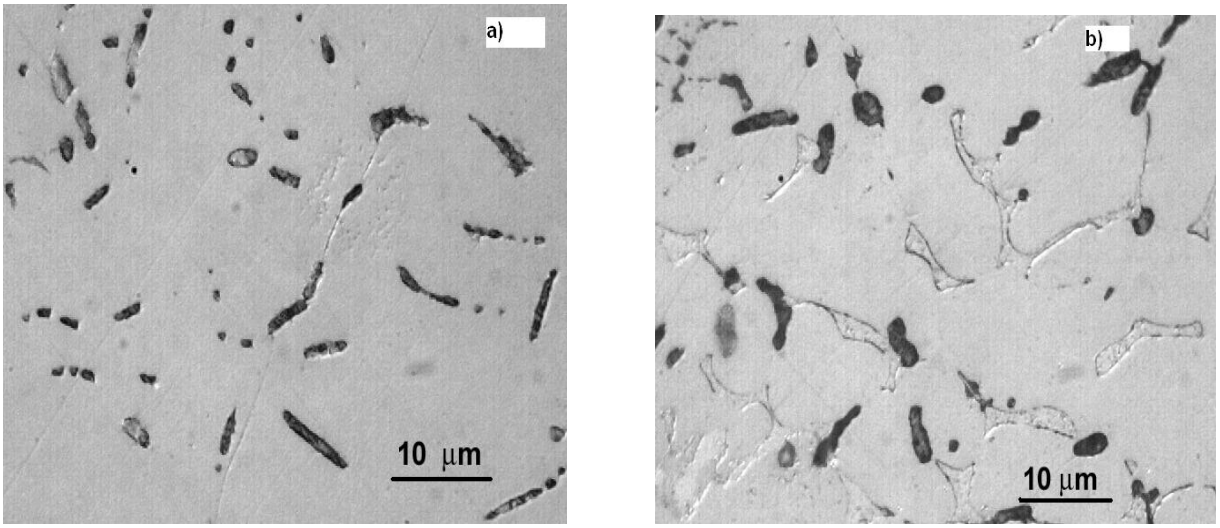

Figure 1. Micrograph of Ni-Al-Cu intermetallic alloys containing a) 20% and b) 25% Cu.

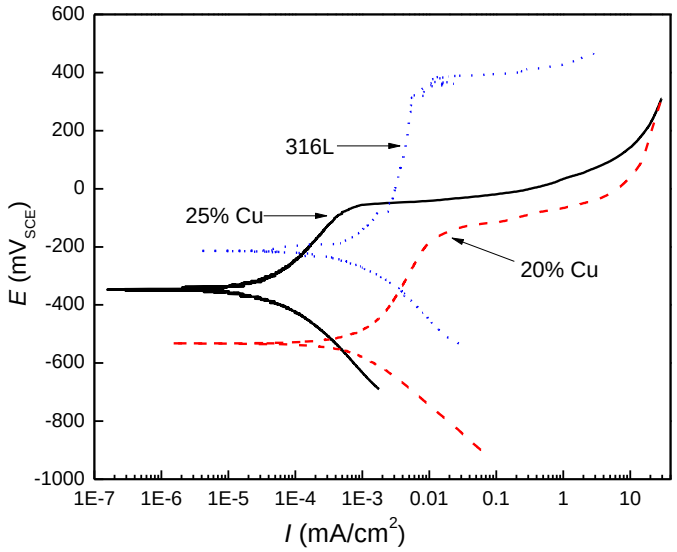

Figure 2. Effect of Al content on the polarization curves for Ni-Al-Cu intermetallic alloys in Hank´s solution.

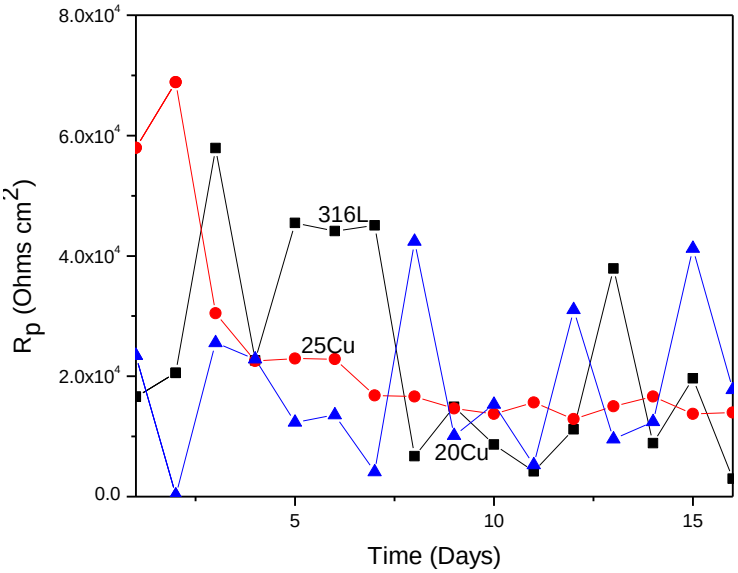

Figure 3. Effect of Al content on the change in the R_p value with time for Ni-Al-Cu intermetallic alloys in Hank´s solution.

Table 3. Electrochemical parameters obtained from polarization curves

Material	E_{corr} (mV_{SCE})	i_{corr} (mA/cm^2)	E_{pit} (mV_{SCE})	i_{pp} (mA/cm^2)
316L	-211	1.5×10^{-3}	330	4.6×10^{-3}
M1	-349	2.75×10^{-5}	109	1.47×10^{-4}
M2	-532	6.94×10^{-4}	-160	3.6×10^{-3}

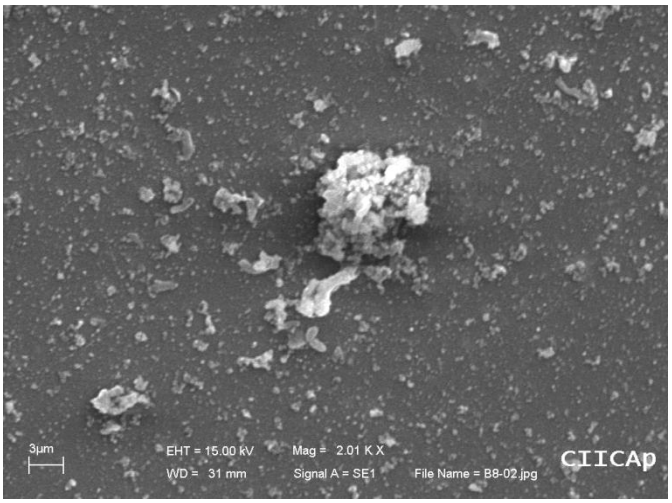

Figure 4. Micrograph of specimen containing 20% Cu corroded in Hank´s solution before removing corrosion products.

The variation of the polarization resistance value with time, R_p, for the different alloys is shown on Fig. 3, which shows that at the beginning of the experiment, the alloy containing 25% Cu had the highest R_p value, higher than the values obtained for 316L type stainless steel and the alloy containing 20% Cu. However, the R_p value for the 25% Cu-containing alloy dropped drastically and remained more or less constant as time elapsed, whereas the same value for the 20% Cu-containing alloy followed an erratic behavior with time.

On the other hand, the R_p value for 316L type stainless steel increased with time reaching values up to four orders of magnitude higher than those obtained for the Cu-containing alloys, decreasing towards the end of the test, reaching similar values to those obtained at the beginning of the experiment. This behavior can be explained in terms of the stability of the external formed corrosion products layer: if this layer is very stable, and it is not detached from the metal surface, the R_p value remains more or less constant, but if this layer is detached and formed again, the R_p value will be fluctuating as time elapsed. After an initial erratic behavior, the R_p value for 316L type stainless steel decreased and showed a more or less constant value. During the last five days or so, the Cu-containing alloys exhibited very similar R_p values, and thus, similar corrosion rates, indicating a lower corrosion resistance of the two Cu-containing alloys as compared with the commonly used 316L stainless steel.

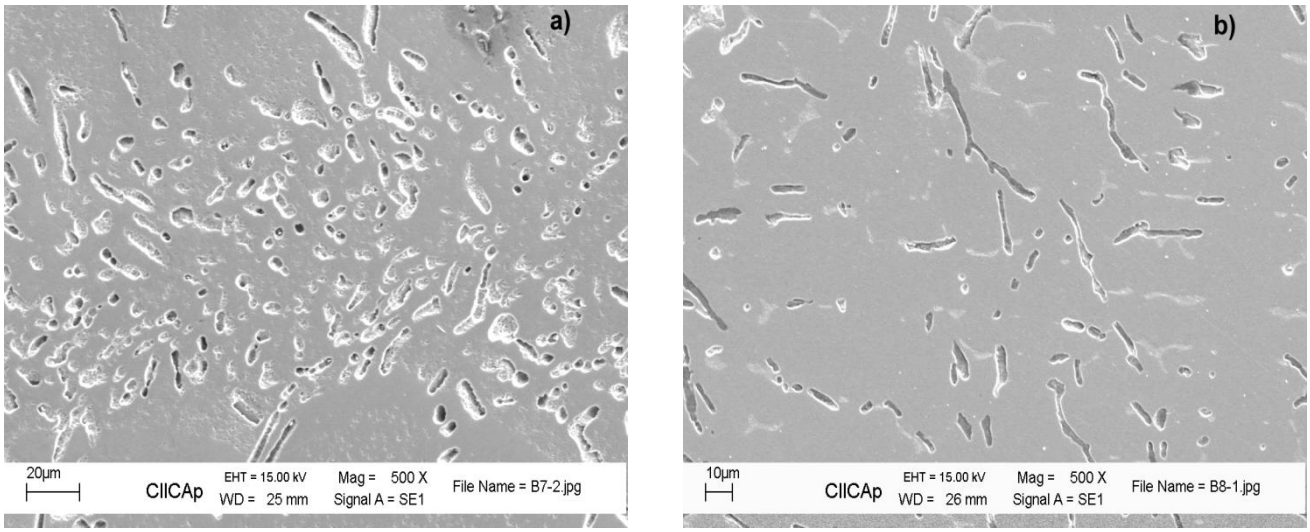

Figure 5. Micrographs of Ni-Al-Cu alloys containing a) 25, and b) 20% Cu exposed to the Hank´s solution after removing corrosion products.

An SEM micrograph of corroded specimen containing 20% Cu before removing the corrosion products can be observed in Fig. 4, showing a compact film, without evidence of porous or micro cracks which allow the diffusion of electrolyte. Once the corrosion products have been removed from the corroded specimens, they had an appearance as shown on Fig. 5 which shows that the different intermetallic alloys suffered from a pitting type of corrosion, where the γ'-$(Ni, Cu)_3Al$ phase was preferentially corroded whereas the β-(Ni, Cu)Al phase remained undamaged.

EIS data in both Nyquist and Bode formats for 316L type stainless steel at different exposure times are shown on Fig. 6. Nyquist diagram show that the data describe two depressed, capacitive-like

semicircles, Fig. 6 a, with their centers in the real axis: one at high frequencies and another at intermediate and lower frequency values. The high frequency semicircle is related to the double electrochemical layer, whereas the lower frequency semicircle is related to the passive layer, probably a Cr_2O_3 oxide, just as evidenced by polarization curves shown on as shown on Fig. 2 indicating that the corrosion process was under charge transfer control. The semicircle diameter has been related with the charge transfer resistance, R_{ct}, equivalent to the polarization resistance R_p in the Stern-Geary equation. Thus, an increase in the semicircle diameter means a decrease in the corrosion rate. It can be seen from Fig. 6 that the semicircle diameter increased during the first few days, but after this time, the diameter decreased. This means that the corrosion rate decreased during the first days, but later it increased.

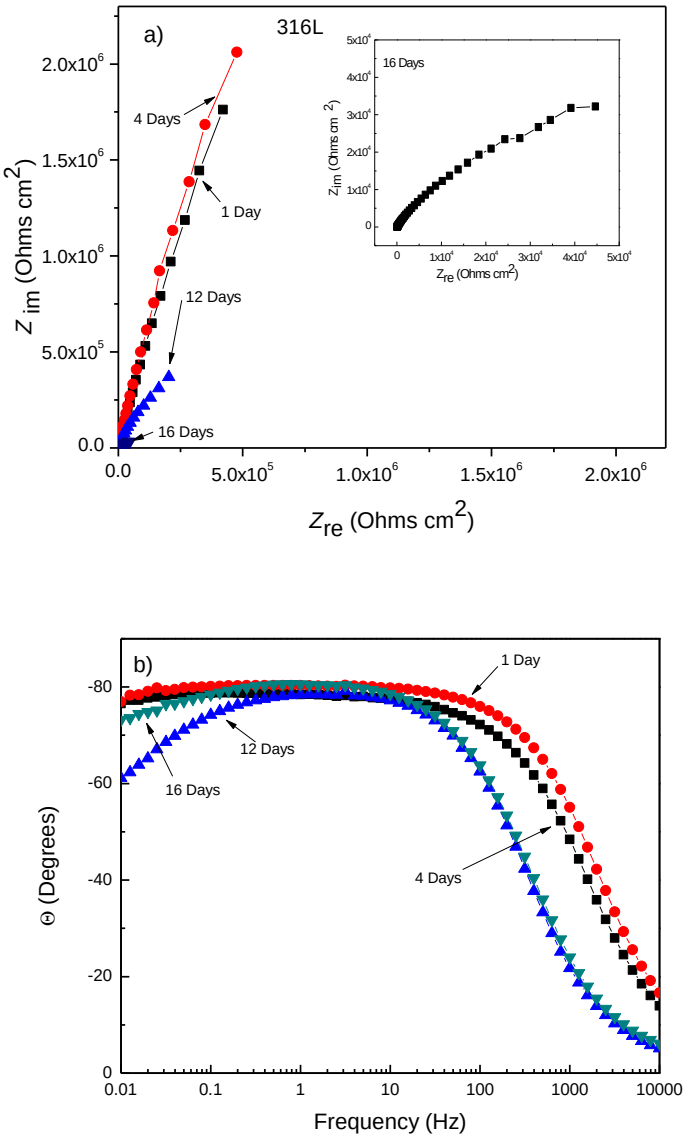

Figure 6. a) Nyquist and b) Bode diagrams for 316L stainless steel in the Hank´s solution after different exposure times.

On the other hand, Bode-phase diagram shown on Fig. 6 b shows two time constants in all cases; a highly capacitive behavior, typical of passive materials, is indicated from medium to low frequencies by phase angles approaching -90°, suggesting that a very stable film is formed on 316L type stainless steel in the used electrolyte.

EIS data for Ni-Al-25Cu intermetallic alloy in the Nyquist format, shown on Fig. 7 a, shows the presence of two depressed, capacitive-like semicircles: one at high frequency values, related to the double electrochemical layer, indicating that the corrosion process was under charge transfer control from the alloy to the electrolyte; a second semicircle was present at intermediate and lower frequencies, related to a passive layer, probably a mixture of NiO, Al_2O_3 and CuO oxides, as evidenced in the polarization curves for this alloy on Fig. 2 and micrographs shown in Fig. 4.

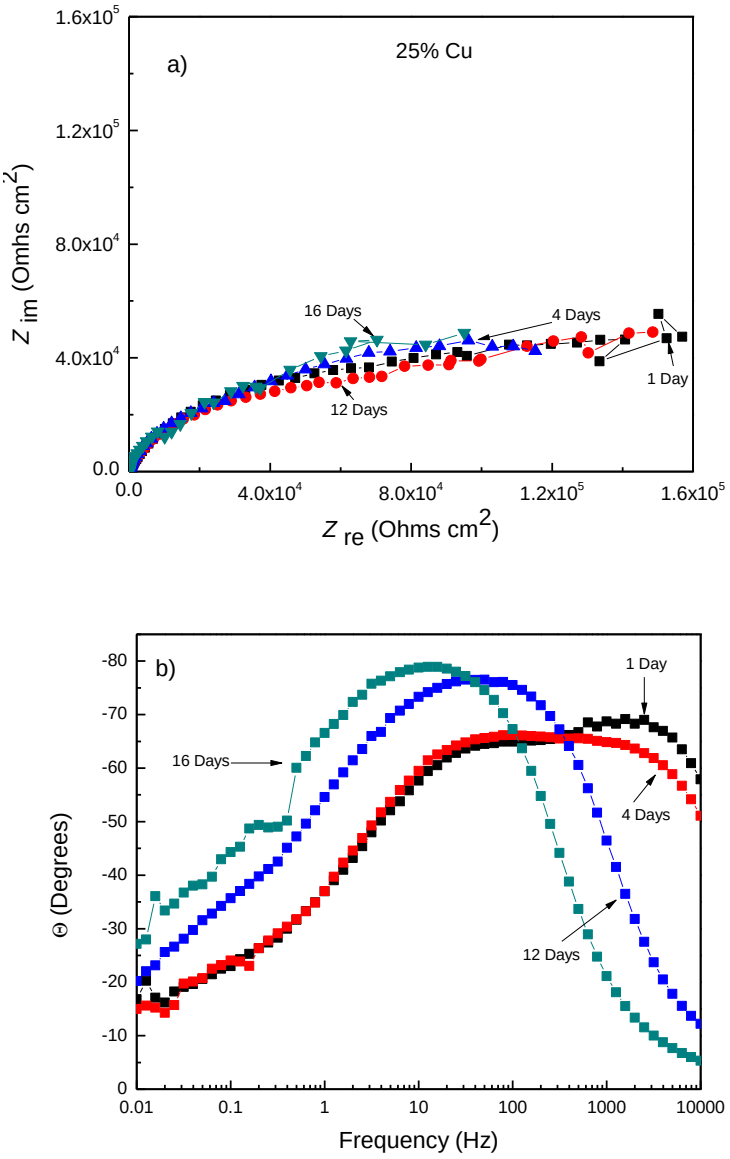

Figure 7. a) Nyquist and b) Bode diagrams for Ni-Al-Cu intermetallic alloy containing 25% Cu in Hank´s solution after different exposure times.

It can be seen that the semicircle diameter was almost 5 times lower than the corresponding values obtained for 316L stainless steel. Bode diagram, on the other hand, Fig. 7 b, shows two time constants during the first 4 days or so, but after this time, the peaks are shifting towards lower frequency values, and the frequency interval that these two time constant were present was narrowed, indicating the lower stability of the passive film as compared to that present on 316L stainless steel.

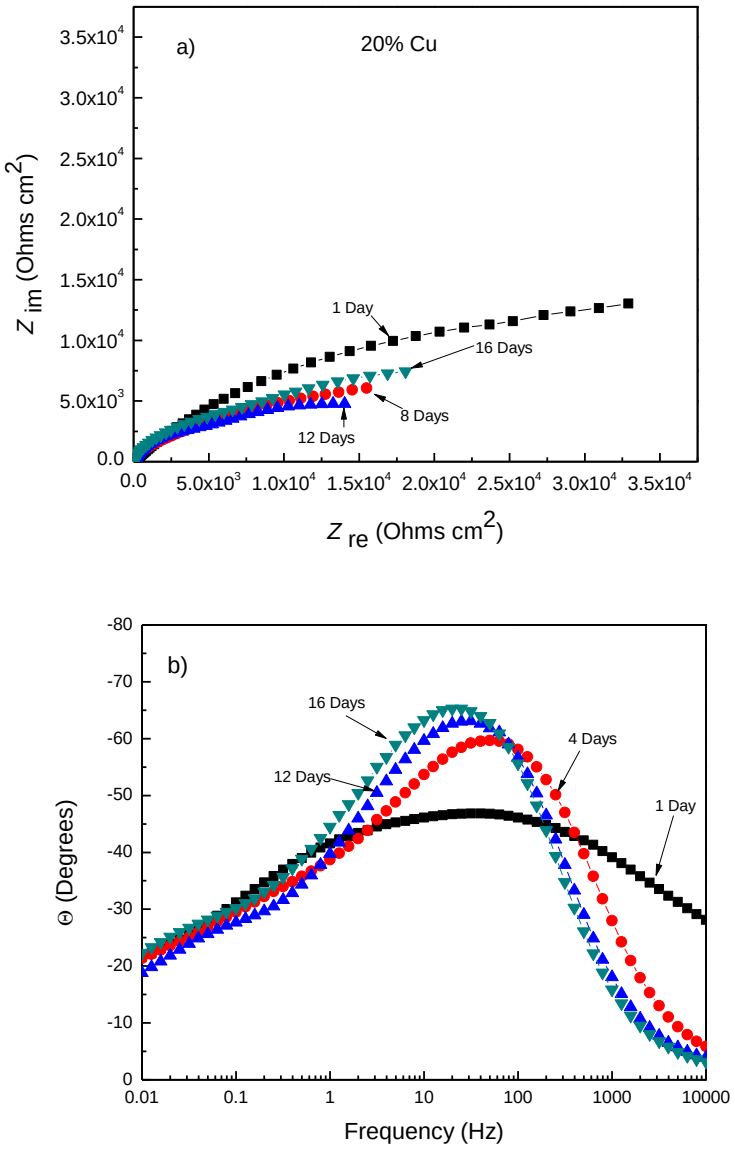

Figure 8. a) Nyquist and b) Bode diagrams for Ni-Al-Cu intermetallic alloy containing 20% Cu in Hank´s solution after different exposure times.

The semicircle diameter values were much smaller than those shown by the 25Cu-containing Ni-Al alloy and the 316L stainless steel, indicating a higher corrosion rate for this alloy. The semicircle diameter was maximum during the first day, it decreased after a few days, and then it

increased again at longer exposure times, indicating a very unstable film, as it was evidenced by the change in the R_p values with time shown on Fig. 3. Bode diagram for this alloy, Fig. 7 b, showed two time constant values only during the first day of testing, however, as time elapsed, only one time constant was present, indicating the low stability of the external formed passive layer.

Table 4. Calculated parameters to simulate the EIS data for the different alloys tested after 1 day.

Material	R_s(Ohm cm^2)	Y_{dl} (Ohms^{-1} cm^{-2} s^n)	n_{dl}	R_{dl}(Ohm cm^2)	Y_f (Ohms^{-1} cm^{-2} s^n)	n_f	R_f (Ohm cm^2)
M1	20	3.12 X 10^{-6}	0.86	288	1.48 X 10^{-5}	0.40	52759
M2	21	8.57 X 10^{-6}	0.76	94	9.04 X 10^{-5}	0.67	34537
316L	41	8.09 X 10^{-6}	0.85	578	1.46 X 10^{-5}	0.84	62464

Table 5. Calculated parameters to simulate the EIS data for alloy M2 at different immersion times.

Day	R_s(Ohm cm^2)	Y_{dl} (Ohms^{-1} cm^{-2}s^n)	n_{dl}	R_{dl}(Ohmcm^2)	Y_f (Ohms^{-1} cm^{-2} s^n)	n_f	R_f (Ohm cm^2)
1	21	8.57 X 10^{-6}	0.76	94	9.04 X 10^{-5}	0.67	34537
4	23	1.07 X 10^{-5}	0.66	114	4.04 X 10^{-5}	0.47	24501
8	25	2.13 X 10^{-5}	0.83	1652	1.23 X 10^{-4}	0.41	35660
12	22	2.45 X 10^{-5}	0.85	2545	1.54 X 10^{-4}	0.41	13044
16	19	2.52 X 10^{-5}	0.86	2753	1.26 X 10^{-4}	0.41	15426

Nyquist diagram for the Ni-Al-20Cu, Fig. 8 a, shows, again, the presence of one depressed, capacitive-like semicircle at high frequency values, related to the double electrochemical layer, and a second semicircle present at intermediate and lower frequencies, related to the presence of a passive layer, as evidenced by polarization curves on Fig. 2. The semicircle diameter was much smaller than those shown by 316L stainless steel and the 25Cu-containing alloy. Bode diagrams for the Ni-Al-20Cu, Fig. 8 b, showed two time constants only during the first day, but for longer times than this, only one time constant was present, indicating the low stability of any formed film on this alloy. Comparing Nyquist diagrams for the three alloys, it can be seen that the highest semicircle diameter, and thus the lowest corrosion rate, was shown by 316L type stainless steel, but towards the end of the test, this value decreased, increasing the corrosion rate.

Equivalent electric circuits used to simulate the EIS data is shown in Fig. 9, where R_s represents the solution or electrolyte resistance, R_{dl} is the double electrochemical layer resistance associated to the charge transfer resistance and C_{dl} its capacitance, R_f is the resistance of the film associated to the participation of corrosion products and C_f its capacitance. When a non-ideal frequency response is present, it is commonly accepted to employ distributed circuit elements in an equivalent circuit. The most widely used is constant phase element (*CPE*), which has a non-integer power dependence on the frequency. The impedance of a CPE is described by the expression:

$$Z_{CPE} = Y^{-1} (j\omega)^{-n} \quad (1)$$

where Y is a proportional factor, j is $\sqrt{-1}$, ω is the frequency and $-1 < n < 1$ has the meaning of a phase shift. Often a *CPE* is used in a model in place of a capacitor to compensate for non-homogeneity in the system. Calculated parameters to simulate the EIS data for different intermetallic alloys are shown on table 4. It can be seen that the resistance of the barrier layer associated to the participation of corrosion products, R_f, is, in all cases, significantly higher than the resistance of the double electrochemical layer, $R_{dl.}$ This indicates that the protection is mainly given by the inner barrier layer, as also provided in the literature [23, 24]. The R_f value for alloy M2, as given on table 5, showed an erratic behavior during the first days, which means that the film formed by corrosion products, for instance NiO or Al_2O_3 oxides, even a biofilm, increases in thickness and then it decreases after some time. After twelve days or so, this formed film is stabilized as observed by the stable values in R_f, giving lower values than those observed during the first days, indicating an increase in the corrosion rate by alloy containing 20% Cu in this environment.

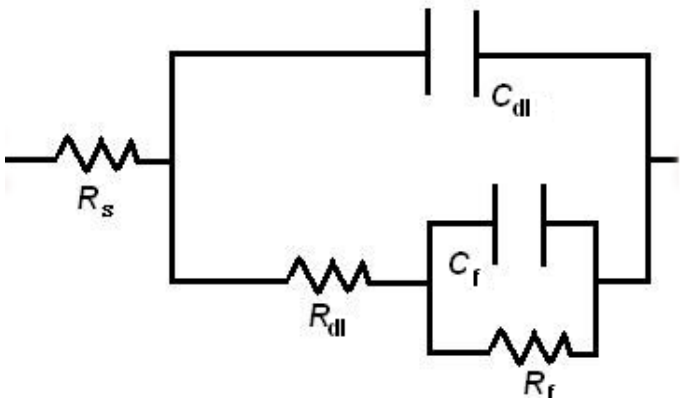

Figure 9. Electric circuit used to simulate the EIS data for tested materials.

To have an insight towards the susceptibility than the two Cu-containing alloys could show towards any type of localized corrosion such as pitting, some electrochemical noise tests in current were carried out. The time series for the electrochemical noise in current for the Ni-Al-25Cu alloy after different exposure times are shown on Fig. 10. It can be seen that after one day of exposure, the times series showed anodic and cathodic transients with high frequency and low intensity, characteristic of a materials which is passivated, but this passive layer is broken and the underlying alloy is corroded, showing an increase in the current. Once the passive layer is re-established, the current decreases. Thus, these transients represent passive layer rupture-repassivation events, e.g. pitting initiation. As time elapsed, both the intensity and frequency of these transients increased, indicating a higher pitting susceptibility of the alloy, and, thus, an unstable passive layer. For the Ni-Al-20Cu alloy, Fig. 11, the time series at the beginning of the experiment showed transients of low intensity and low frequency, indicating the onset of a localized type of corrosion, but as time elapsed,

the intensity and frequency of the transients increased, indicating an increase in the susceptibility towards a localized type of corrosion.

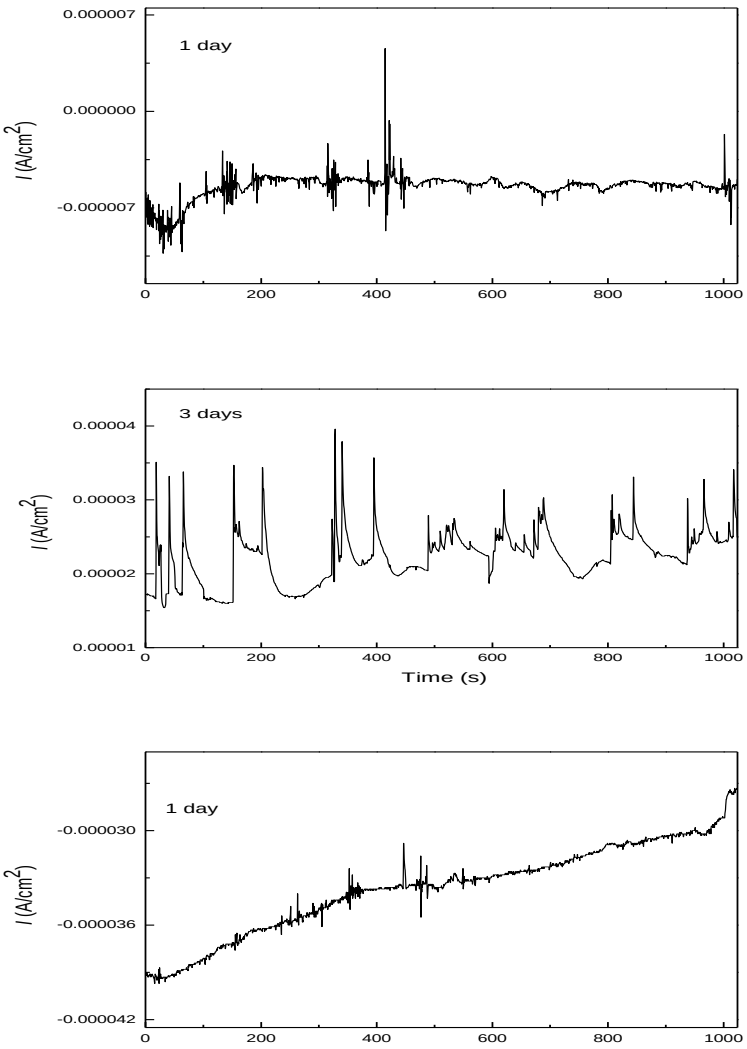

Figure 10. Noise in current for Ni-Al-Cu intermetallic alloy containing 25% Cu in Hank´s solution.

This behavior is more clearly observed in the power spectral density analysis using the fast Fourier transformation, as shown in Fig. 12, where it can be seen that, for the same frequency, the highest intensity in current transients was shown by the specimen containing 20%Cu after 8 days of exposure to the corrosive environment, and the lowest intensity was shown by the specimen containing 25% Cu after 1 day of exposure.

By using the potential noise standard deviation, σ_v, and dividing it by the current noise standard deviation, σ_i, we can obtain the noise resistance, R_n, and its change with time for the different intermetallic alloys, Fig. 13. It can be seen that, although there is a severe fluctuation of data and is hard to make any comparison, generally speaking, the highest R_n value was for the alloy with the

highest Cu content, and it decreased as time elapsed, showing an erratic behavior as time elapsed. This behavior was very similar to what was exhibited by R_p, Fig. 3. Thus, we can see that the noise resistance value, R_n, gives information about the corrosion rate in the same way as R_p doest. Thus, by using any analysis tool, alloy containing 25% Cu showed the highest corrosion resistance.

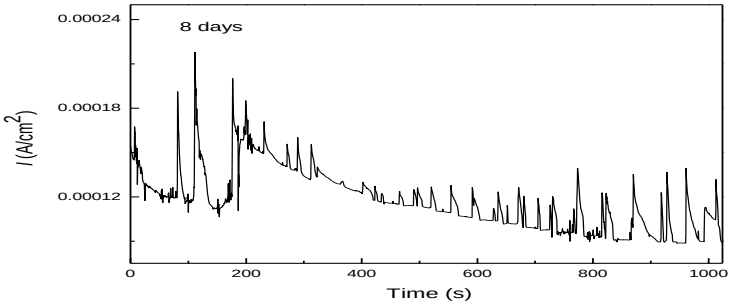

Figure 11. Noise in current for Ni-Al-Cu intermetallic alloy containing 20% Cu in Hank´s solution.

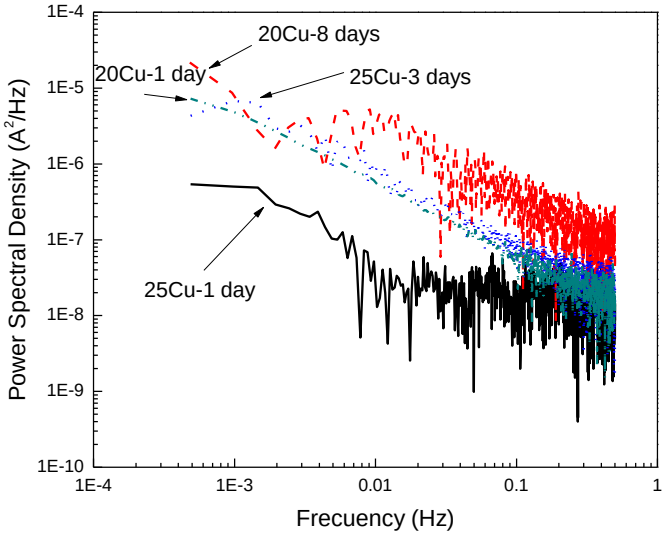

Figure 12. Power spectral density plots for the two Ni-Al-Cu intermetallic alloys in Hank´s solution.

In general terms, it has been shown that the resistance to uniform corrosion in Ni-Al type aluminides decreased by alloying them with Cu. As the Cu content increased, the uniform corrosion resistance increased as evidenced by polarization curves and LPR results, but also the tendency towards localized, pitting-like corrosion decreased. Thus, the γ'-$(Ni, Cu)_3Al$ phases were the most susceptible towards pitting type of corrosion. This can be explained in terms of the galvanic effect, since the γ'-$(Ni, Cu)_3Al$ phases acted as anode, whereas the β-(Ni, Cu)Al phases acted as cathodes, therefore the γ'-$(Ni, Cu)_3Al$ phases were very susceptible to localized of corrosion. Polarization curves have shown that Ni-Al-Cu intermetallic alloys could be passivated in human body environments.

However, the erratic behavior in the R_p, *and* R_n values has shown that this protective passive film can be detached from the surface, leaving the substrate unprotected against the corrosive environment.

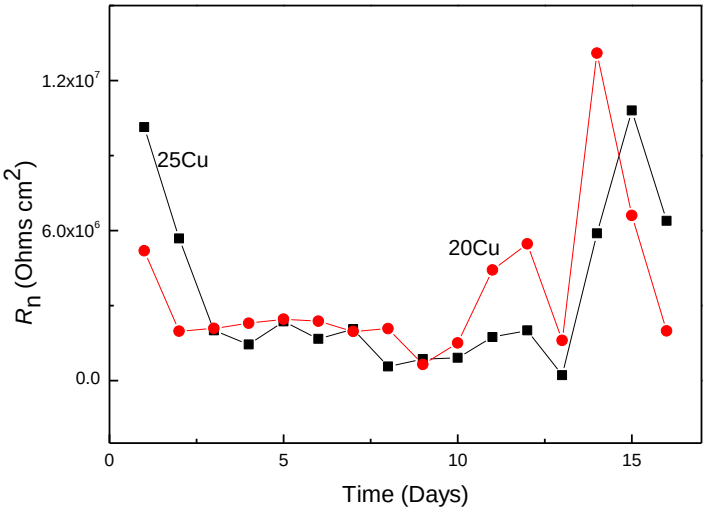

Figure 13. Effect of Al content on the change in the noise resistance value with time, R_n, for Ni-Al-Cu intermetallic alloys in Hank´s solution

This film can be either in the whole surface or in some localized places, especially in presence of chlorides, like in the present cases, allowing aggressive ions to attack the alloy in these unprotected places, inducing pitting type of corrosion. Since the most susceptible phases, the γ'-$(Ni, Cu)_3Al$ ones, acted as anodes, these were the preferential places for pitting corrosion to occur. Normally, additions of Cu have been reported to increase the corrosion resistance of iron-base alloys in acidic solution, sea water and alkaline solutions [21]. This corrosion resistance has been reported to be due to the establishment a more stable passive layer. Frangini [25] has shown that additions of some ternary elements to NiAl intermetallics such as Cr or Ti improve the Al_2O_3 protectiveness by suppressing detachment of these scales. Additionally, they showed that, if Cu is added, there will be some diffusion outwards of Cu rather than inwards diffusion of Al, thus, preventing the formation of voids on the surface that could lead to a scale detachment. The increased corrosion resistance has been reported to be due to the establishment a more stable passive layer in addition to the formation of voids as explained above. [26, 27] If the relative contents of Ni into the passive layer decrease, by increasing the Cu contents in the alloy, the improvement of the passive Al_2O_3 layer is loosened.

4. CONCLUSIONS

The corrosion behavior of Ni-Al-Cu intermetallic alloys as possible materials to be used in human body environments has been evaluated. Generally speaking, all results have shown that their corrosion resistance was lower than that for conventional 316L type stainless steel. This corrosion resistance decreased with time and as the Cu content decreased in the alloy. The erratic change in the

linear polarization and noise resistance values, R_p and R_n, indicated that the passive film on the alloys could be detached from the surface inducing a localized, pitting type of corrosion in preferential places such as γ'-$(Ni, Cu)_3Al$ phases. EIS measurements showed that in alloys containing Cu, the corrosion process was under charge transfer control.

References

1. J.J. Jacobs, J.L. Gilbert and R.M. Urban, *J. Bone Joint Surgery* 80A (1998) 268.
2. A.Choubey, B. Basu and R. Balasubramaniam, *Trends Biomater: Artif Organs* 18 (2005) 64.
3. F. Barragan, R. Guardian, C. Menchaca, I Rosales, J. Uruchurtu, *Int. J. Electrochem. Sci*. 5 (2010) 1799-1809
4. Madhuav Prasad Neupanc, Il Song Park, Sook Jeong Lee, Kyoung A Kim, Mia Ho Lee, Tae Sung Bae, *Int. J. Electrochem. Sci*. 4 (2009) 197-207
5. J.A.Ruiz, I.Rosales. J.G. Gonzalez-Rodriguez, J. Uruchurtu. *Int. J. Electrochem. Sci*. 5(2010) 593-604.
6. T.M. Sridhar, U.K. Mudali and M. Subbaiyan, *Corros. Sci*. 45 (2003) 237.
7. Y.L. Zhou, M. Ninomi, T. Akahori, H. Fukui and H.Toda, *Mat. Sci. Eng.* 398A (2005) 28.
8. R.W.Y. Poon, J.P.Y. Ho, X. Liu and C.Y. Chung, *Mat. Sci. Eng*. 390A (2005) 444.
9. F.T. Cheng, K.H. Lo, H.C. Man, *J. Alloys Compounds* 437 (2007) 322.
10. Y.F. Zheng, B.L. Wang, J.G. Wang, C. Li, L.C. Zhao, *Mat Sci Eng* 438A (2006) 891.
11. Y.H. Li, G.B. Rao, L.J. Rong, Y.Y. Li and W. Ke, *Mat Sci Eng* 363A (2003) 356.
12. M. Metikos-Hukovic and R Babic, *Corros. Sci*. 49 (2007) 3570.
13. M. Metikos-Hukovic and R. Babic, *Corros. Sci*. 51(2009) 70.
14. M. Clesic, W. Reczyski, A.M. Janus, K. Engvall, R.P. Socha and A. Kotarba *Corros. Sci.* 51(2009)1157.
15. J.H. Chern Lin, K.S. Chen and C.P. Ju, *Mat. Chem. Phys*. 41(1995) 282.
16. W.Y. Guo, J. Surr and JS Wu, *Mat. Chem. Phys*. 113 (2008) 616.
17. M.C. Garcia-Alonso, M.F. Lopez, M.L. Escudero, J.L. Gonzalez-Carrasco and D.G. Morris, *Intermetallic*s 7(1999)185.
18. M.F. Lopez, M.L. Escudero, E. Vida, A.R. Pierna and F.F. Marzo, *Electrochim. Acta* 42 (1997) 659.
19. M.F. Lopez, A. Gutierrez, M.C. Alonso-Garcia and M.L. Escudero, *J. Mater. Res*. 13(1998) 3144.
20. G. Sharma, K.B. Gaonkar and P.R. Sing, *Materials Letters* 61 (2007)971.
21. D.B. Miracle and R. Darolia, in: J.H. Estbrook, R.L. Fleisher (eds) Intermetallic Compounds: Principles and Practice, Whiley, (1995) New York.
22. G.R. Bozzolo, D. Noebe, F. Honey, *Intermetallics* 8(2000) 7.
23. N.J. Medvedeva, Y.N. Gornostyrev, D.L. Novikov, O.N. Myrasov and A.J. Freeman, Acta *Metall. Mater*. 46(1998) 3433.
24. Y.L. Zhou, M. Ninomi, T. Akahori, H. Fukui and H. Toda, *Mat. Sci. Eng*. 398A (2005) 28.
25. Frangini S, Masci A (2004) *Surf Coatings Technol* 184:31
26. D.Q. Martins, W.R. Osorio, M.E.P. Souza, R. Caram and A. Garcia, *Electrochim. Acta* 53 (2008) 2809.
27. S.J. Lee, S.I. Pyun, *J. Solid State Electrochem* 11 (2007) 829.